Phonon wave-packet simulations using the quantized definition of energy and a temperature-dependent phonon dispersion relation and phonon density of states

Amir Behbahanian ● and Nicholas A. Roberts*

Department of Mechanical and Aerospace Engineering, Utah State University, Logan, Utah 84322-4130, USA

Wave-packet simulations, regarded as phonon dynamics in the literature, have been used to explore interface conductance problems and to study the frequency-based dynamics of systems of particles. In this work we introduce an extension of the method to improve the postsimulation analysis and to add an energy aspect to the definition of a wave packet. In a wave-packet simulation the most populated frequency activated with the wave packet is known through knowledge of the wave number implemented in the atom displacement equation. The one-to-one correspondence of wave number and frequency is known through the phonon dispersion relation (PDR). We add the temperature dependence of this one-to-one correspondence to the analysis of wave packets through consideration of a temperature-dependent PDR and showed the importance of the temperature-dependent PDR in the wave-packet definition by presenting results considering and neglecting the phenomenon. In addition, the temperature-dependent PDR and the density of states provide us the chance to change the nature of the atomic displacement amplitude as an arbitrary parameter to a tuning knob for the amount of energy it carries and utilize the chance to provide a quantitative measure for the validity of molecular-dynamics simulations considering their classical nature in comparison with the quantum particle picture of phonons.

I. INTRODUCTION

Material selection and material engineering have been shown to be promising approaches to overcome design bottlenecks in multiple engineering disciplines dealing with thermal or lattice-vibration-related problems. The target properties are achieved either through designing new materials that do not exist in nature [1] or through a better understanding of the physics of existing materials. Increasing the thermal conductivity at an interface for the sake of controlling the temperature below the maximum operational temperature of electronics, decreasing the thermal conductivity to increase the figure of merit in thermoelectric systems, and finally increasing the coupling in mechanical resonators to approach better sensing capabilities are the most common applications that will benefit from a better understanding of thermal transport properties in materials [2–4]. Analytical and computational modeling are considered effective tools to characterize the physics of the existing materials.

Both computational and analytical approaches are categorized into two main streams: (i) equilibrium analysis and (ii) nonequilibrium analysis. The Boltzmann transport equation (BTE)–based simulations and Green-Kubo simulations are the main equilibrium approaches to provide the frequency-based behavior of a material. Singh *et al.* used the BTE approach to calculate the relaxation time and, as a result, the conductance across the Si/Ge interface [5] and Lv and Henry proposed a Kubo-based approach for the exploration of the mode-mode contribution to thermal conductivity and performed a case study of amorphous and crystalline silicon [6]. Analytical

approaches in the category of equilibrium analysis are the Green's-function analysis and *n*-phonon interaction analysis based on the radiative heat flux analysis approach [7,8]. These are techniques that have been proven to provide detailed results in frequency space. One other method that is not as ubiquitous as the methods mentioned above is the frequency-based transmission analysis performed by Chalopin and Volz. This analysis provides comprehensive frequency-based transmission across the Si/Ge interface in the specular regime [9].

In addition, the wave-packet creation method is a nonequilibrium method used to study interface transport and can look at the dynamics of a frequency band in a system of particles. This technique of creating wave packets is called phonon dynamics [2] and the method was proposed by Schelling *et al.* [10]. It is based on the creation of a sinusoidal wave, which is in a Gaussian envelope. The created wave travels in the defined system and by monitoring the dynamics of the motion can provide characteristics such as phonon transport properties and phonon boundary transmission. Schelling and co-workers and Wei *et al.* used the method to calculate the transmission across twist grain boundaries [11,12] and to explore the heat transfer mechanisms of graphene along the in-plane direction [13]. The method was proven to provide reliable and accurate results for transmission across an interface, time-dependent energy distribution, scattering, and phonon lifetime calculations [14,15]. Landry and McGaughey also used the results for validation [16]. The phonon dynamics has always been used assuming an arbitrary constant for the amplitude of a wave packet as a result; the direct effect of the wave-packet amplitude on the amount of energy it carries has been neglected.

A phonon counting process is an essential part of most of the mentioned analyses. As a result, a correct definition of the

*nick.roberts@usu.edu

043311-1

phonon density of states (DOS) is correlated to any subsequent analysis. The use of the DOS in thermal conductivity calculations started with Callaway's linear consideration of the DOS and was reused by other researchers [17,18]. The full-Brillouin-zone consideration of the DOS provided results that matched the experiment better [19]. Still, a nonlinear (frequency-dependent phonon group velocity) full-zone consideration of the DOS provided a more realistic model of materials. Aksamija and Knezevic [20] considered a nonlinear and full-zone DOS and were able to capture the dependence of graphene nanoribbon thermal conductivity on the chiral angle of the ribbons. They also performed the same analysis on silicon-on-insulator nanomembranes and observed the anisotropy of thermal conductivity in these materials. Despite the possibility, the temperature dependence of the DOS was never addressed in computational thermal property calculations, although the decrease of the range of lattice-vibration frequencies with increasing temperature is an accepted and experimentally observed phenomenon in physics research [21,22]. This phenomenon was attributed to the coupling of optical and acoustic phonons [23] or the electron-phonon interactions [24]. Typically, the temperature dependence of the calculation is solely based on the temperature dependence of the Bose-Einstein distribution [25,26], although the importance of the temperature-dependent DOS and phonon dispersion relation (PDR) was recently addressed by Gerboth and Walker in the context of size-dependent softening of nanoribbons [27].

The phonon dynamics has always utilized the 0 K DOS and PDR and in its definition the selection of the displacement amplitude is arbitrary. The introduction of the energy to the definition of a wave packet is addressed in this work through consideration of the temperature-dependent DOS and PDR. We use a Green's-function-based definition of the temperature-dependent DOS and the PDR [28] in order to get the energy of a frequency band. The frequency space of the wave packet created using the mentioned approach is tested using a Fourier-analysis-based method to provide the difference between considering the temperature dependence and ignoring it. In addition, knowledge of the energy of a wave packet based on the quantum definition of phonons provides the chance to quantitatively check the extent of the validity of molecular-dynamics (MD) simulations in frequency space and at different temperatures.

To present the details of the work, we first elucidate the details of the computational approaches for the calculation of the PDR and the DOS $g(\omega)$ followed by the methodology to capture the correct kinetic energy of a wave packet. The system, which is the test specimen to simulate and validate the proposed methodology, is defined in Sec. II. We present our results and discuss the uncertainty of the numerical calculations in Sec. III. We summarize in Sec. IV.

II. METHODS

We designed an extension of the phonon dynamics method that captures the correct kinetic energy of a frequency band in a wave packet, which results in a wave packet carrying the same amount of energy at a specific temperature in the frequency band flowing in a specific Cartesian direc-

tion. The definition of the energy is based on the quantum definition of energy for the range of frequencies within a frequency band in a Gaussian envelope. For the temperature-dependent definition of the energy in any system we require the temperature-dependent definition of the PDR and the DOS. In this section we start with the definition of the PDR and the DOS and then we define the methodology to structure a wave packet considering the temperature-dependent definition of the PDR and the DOS.

A. Phonon dispersion relation and density of states

We encountered two computational methods that can capture the temperature dependence of the PDR and are able to capture the full anharmonic picture of the dynamics. The first approach was proposed by Heino [29], which is based on mapping the velocity field to the k space ($k = \frac{2\pi}{\lambda}$) and getting the spatial Fourier transform of the velocity field $v^\alpha(t, r)$, where α indicates the direction in the coordinate system for each particle indexed with i. The calculation is followed by the computation of the autocorrelation function $A^\alpha(k, t)$ of the k-space velocity vectors. As a result, the PDR is the output of the temporal Fourier transform over the total simulation time T_{sim} of $A(k, t)$, which provides the autocorrelation function as a function of angular frequency ω and k vectors [$A(k, \omega)$]

$$v^\alpha(k, t) = \sum_i v_i^\alpha(t, r)e^{-ikr_i},$$

$$A^\alpha(k, t) = \frac{\langle v^\alpha(k, t) \cdot v^\alpha(k, 0)\rangle}{\langle v^\alpha(k, 0) \cdot v^\alpha(k, 0)\rangle},$$

$$A^\alpha(k, \omega) = \sum^{T_{sim}} A^\alpha(k, t)e^{-i\omega t}. \tag{1}$$

The second method is a particle tracking model and defines the dynamical matrices $D(k, \omega)$ in the context of atom positions over time [28,30]. This method first maps all the α components of the atom positions at each time t, $R_{i\alpha}(x, t)$, in the k space by a spatial Fourier transform. The sum is over the location of each primitive cell [Fig. 1(a)] in the primitive structure, but it reduces to a summation over atoms i as we have one atom per unit cell, due to the distribution of atoms along the primitive lattice vectors,

$$R_{i\alpha}(k, t) = \frac{1}{\sqrt{N}}\sum_i R_{i\alpha}(x, t)e^{-ikr_l}. \tag{2}$$

The force constants matrix elements $\phi_{i\alpha, j\beta}(k)$ are defined with respect to the positions in k space $R_{i\alpha}(k, t)$. The definition is based on defining the Green's function in terms of the time-dependent α and β components of the position of atoms i and j. Here k_b and T are the Boltzmann constant and the simulation temperature, respectively. In the following, the asterisk denotes the complex conjugate of a complex vector:

$$G_{i\alpha, j\beta}(k) = \langle R_{i\alpha}(k, t) \cdot R_{j\beta}^*(k, t)\rangle$$

$$- \langle R_{j\beta}(k, t)\rangle \cdot \langle R_{j\beta}^*(k, t)\rangle,$$

$$\phi_{i\alpha, j\beta}(k) = k_b T \, G_{i\alpha, j\beta}^{-1}(k). \tag{3}$$

As a result, we define the dynamical matrices with the aid of force constant matrices, and the squares of angular
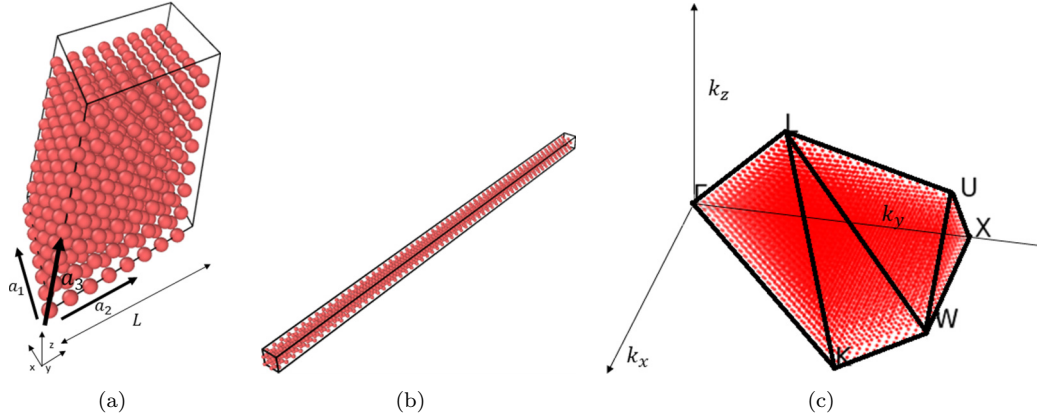
FIG. 1. (a) Primitive structure conducive to the spatial Fourier analysis. (b) Validation system. (c) Volumetric mesh in k space.

frequencies are the eigenvalues of the proper eigenproblem:

$$D_{i\alpha,j\beta}(k) = \frac{1}{\sqrt{m_i m_j}} \phi_{i\alpha,j\beta}(k),$$

$$|D_{i\alpha,j\beta}(k) - \delta_{\alpha\beta}\delta_{ij}\omega^2(k)| = 0. \tag{4}$$

This method, up to the generation of dynamical matrices, is available as FIX-PHONON in the LAMMPS molecular dynamics package [31].

The DOS $g(\omega)$ is the count of frequencies within a frequency bin centered at ω. The width of the frequency bins was chosen to be equal to 0.01 THz. It is also essential to perform the DOS normalization precisely by considering all of the three polarizations p, which results in integration over all frequencies of the $g(\omega)$ being equal to 3:

$$\int_0^{\omega_{\max}} g(\omega)d\omega = \sum_p 1 = 3. \tag{5}$$

The temperature dependence of the PDR and DOS is a phenomenon addressed by other researchers as phonon softening [21]. The frequency shift due to temperature change is also an observable phenomenon in Raman spectroscopy experimental measurements [32]. The change in the frequency behavior of the PDR and softening of the frequencies were attributed to the change of the lattice constant due to thermal expansion [33]. Although the work by Yun *et al.* is on UO$_2$, their observation is relevant to this work on argon as the thermal conductivity of UO$_2$ is lattice dominated up to high temperatures (1400 K) [34], which is well above the temperatures studied in the work by Yun *et al.* [33]. We confirmed this behavior in our system by first running ten different simulations at 50 K with ten different random velocity seeds to capture the numerical oscillation of the results and monitoring the frequency space of the system at the same four different temperatures under the canonical ensemble (NVT); the analysis will ensure the change being beyond the statistical variations.

B. Simulation conditions

Two distinguished systems of particles are defined: (i) for the characterization of the Lennard-Jones argon and (ii) to compare the expected characteristics of a wave packet with the

ones used in the literature neglecting the temperature effects. To achieve a high k-space resolution, in the analysis system, we choose a $40 \times 40 \times 40$ unit cell system in the format of a primitive structure. We model the interatomic interactions with the 6-12 Lennard-Jones potential. The constants of the potential ϵ and σ are 1.69×10^{-21} J and 3.4×10^{-10} m, respectively [35]; as a result, we calculate the lattice constant at 0 K as 5.2411 Å [36]. The run process of the analysis section is a combination of a 5×10^5 time steps of equilibration followed by 9.5×10^6 time steps of calculation for every temperature; each time step is 2 fs. Both equilibration and calculation steps are in an NPT ensemble, which allows for expansion of the system under the thermal stresses. The validation system [Fig. 1(b)] dimensions are $2 \times 60 \times 2$ unit cells in the format of a cubic structure (not unit cell) and the potential constants are the same as the analysis system. Simulations in the validation system are performed for each wave number (5×10^5 time steps with a time-step temporal length of 1 fs) and are all in a microcanonical ensemble (NVE). The temperature dependence is observed in the validation system by applying an expanded lattice constant for every temperature under analysis. The approach helps us run the system at 0 K and while still being able to observe the temperature-dependent PDR. The possibility of observing the frequency-space temperature dependence at 0 K provides us the chance to isolate any other possible reason resulting in a temperature-dependent behavior and validates lattice expansion as the reason for this type of behavior in dielectrics.

To get the averaged lattice constant at each temperature, we run the validation system with no extra wave packets under NPT and the temperature conditions for 5×10^6 time steps and calculate the average lattice constant after the convergence of macrostates. The calculation of the lattice constant is through the calculation of the average of the atom-atom distances over the time of simulations.

C. Wave-packet generation and energy calculation

We define the wave packet as a sinusoidal function in a Gaussian envelope [Fig. 2(a)]. The Gaussian envelope ensures the smooth decay of the oscillation to avoid unwanted vibrations as a result of abrupt spatial changes in atom displacement. We choose the standard deviation s of the Gaussian
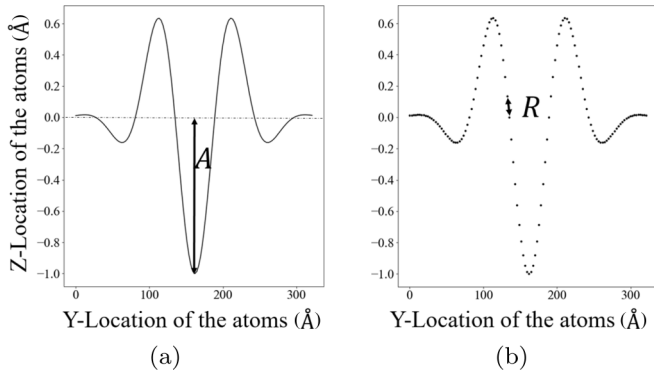
FIG. 2. (a) Representation of a displacement wave. (b) Displacement wave with interatomic distance marked on it.

to be ten times the temperature-dependent lattice constant of argon to get a full wave for wave numbers as low as $\frac{0.1\pi}{a}$, and the Gaussian is centered at the center of the validation system by the definition of μ. The oscillatory part of the displacement function is a simple cosine

$$z(y) = A \exp\left(\frac{(y - \mu)^2}{2s^2}\right) \cos(yk). \tag{6}$$

The exponential definition of oscillation introduces an imaginary part that defines the phase of a hypothetical wave, which is immaterial in the definition of an initial condition.

We apply the displacement to all the atoms in the validation system as a function of the atoms' positions y, which is the direction containing 60 unit cells. To calculate the amplitude of the displacement signal, we first need to define the energy of the wave packet. We calculate the wave-packet energy using the frequency-based kinetic energy E equation. The equation defines the contribution of each angular frequency ω to the energy as the product of the reduced Planck constant and angular frequency $\hbar\omega$. Then the energy in a frequency band (integration between two frequencies) or the total energy (integration over the whole spectrum of frequencies) of the system is the summation of energies considering both the DOS and the Bose-Einstein distribution,

$$E = \int_0^{\omega_{\max}} g(\omega) \frac{\hbar\omega}{1 - \exp(\frac{\hbar\omega}{k_bT})} \, d\omega. \tag{7}$$

Before we apply Eq. (7) to the wave-packet energy calculation, we should note the effect of a Gaussian envelope in real space on the wave, in frequency space. The standard deviation s in real space translates to $1/s$ in frequency space, which requires the consideration of the effect of the Gaussian envelope in the calculation of the kinetic energy of a wave packet. The phenomenon becomes more evident by considering the following:

$$\frac{1}{\sqrt{2\pi s^2}} \int_{-\infty}^{\infty} e^{-x^2/2s^2} e^{i2\pi kx} dk = e^{-2\pi^2 s^2 k^2}. \tag{8}$$

The Gaussian distribution in the frequency space (8) requires us to multiply the energy of the frequency bins, activated by creating a wave packet, by the Gaussian value of the corresponding frequency. The Gaussian in the frequency space is a function of wave number $k(\omega)$ and is centered at

$k'(\omega)$. As a result, the kinetic energy of the entire system between two frequencies ω_1 and ω_2, $E_{\omega_1 \leqslant \omega' \leqslant \omega_2}$, is defined as

$$E_{\omega_1 \leqslant \omega' \leqslant \omega_2} = \int_{\omega_1}^{\omega_2} \left(\frac{e^{s^2[k(\omega) - k'(\omega')]^2}}{\sqrt{2\pi s^2}}\right)$$
$$\times \left(g(\omega)\frac{\hbar\omega}{1 - \exp(\frac{\hbar\omega}{k_bT})}\right) d\omega. \tag{9}$$

The calculated kinetic energy is the kinetic energy of a frequency band flowing in all traveling directions and polarizations. We are interested in the energy of a wave packet traveling in a specific direction. Eigenvectors of the dynamical matrices are usually used to define the flow direction of energy, but the eigenvectors are not continuous in the frequency space and we cannot use them in an integration process. As a result, we define the directional dependence of the energy flow considering the main crystallographic directions. This consideration is supported by the Raman spectroscopy data [37]. Correspondingly, we divide the calculated energy into three sections for each of the three main crystallographic directions in the fcc argon lattice, weighted by the linear atomic density $\mathcal{L}$ in the structure. We calculate the shares of the energy to be 0.47, 0.33, and 0.2 in directions [110], [100], and [111], respectively.

The polarization affects the calculation based on our observation that the creation of a wave by transverse displacement results in the generation of longitudinal modes. We attribute this fact to the creation of a compression field in the crystal in front of a propagating transverse wave. The longitudinal wave has the longitudinal frequency of the same wave number. The observation suggests the need for the addition of the longitudinal energy modes to our energy calculation. As a result, a wave packet carries both the energy of the transverse bandwidth and the energy of the longitudinal contribution. To calculate the energy of each branch contributing to the energy carried by a wave packet, we are required to divide the energy of a frequency bin, calculated by Eq. (9), by 3 if the frequency is less than the maximum frequency of the transverse branch. The same approach has been used with the analytical calculation of thermal conductivity and the contribution of different polarizations [38]. Considering the energy of the frequency band between ω_1 and ω_2, the directional linear atom density $\mathcal{L}_D$, the division of energy based on polarization, and the contribution of different polarization, we can define the total energy of a wave packet $E_{(tot,D)}$. The definition is for two cases, one with frequencies below the maximum transverse frequency $\omega_{T,\max}$ and the other with the frequencies above the maximum transverse frequency,

$$E_{(tot,D)} = \mathcal{L}_D[\tfrac{1}{3}E(\omega'_T) + \tfrac{1}{3}E(\omega'_L)],$$
$$\times \{\omega'_L(k')| \, 0 \leqslant \omega'_L(k') \leqslant \omega_{T,\max}\}$$
$$E_{(tot,D)} = \mathcal{L}_D[\tfrac{1}{3}E(\omega'_T) + E(\omega'_L)],$$
$$\times \{\omega'_L(k')| \, \omega_{T,\max} \leqslant \omega'_L(k') \leqslant \omega_{L,\max}\}. \tag{10}$$

To enforce the kinetic energy on the wave packet, we calculate the interatomic distance R [Fig. 2(b)] based on the Lennard-Jones potential by equating the potential equation to the value of the potential $P_{\max}$ at the bottom of the potential
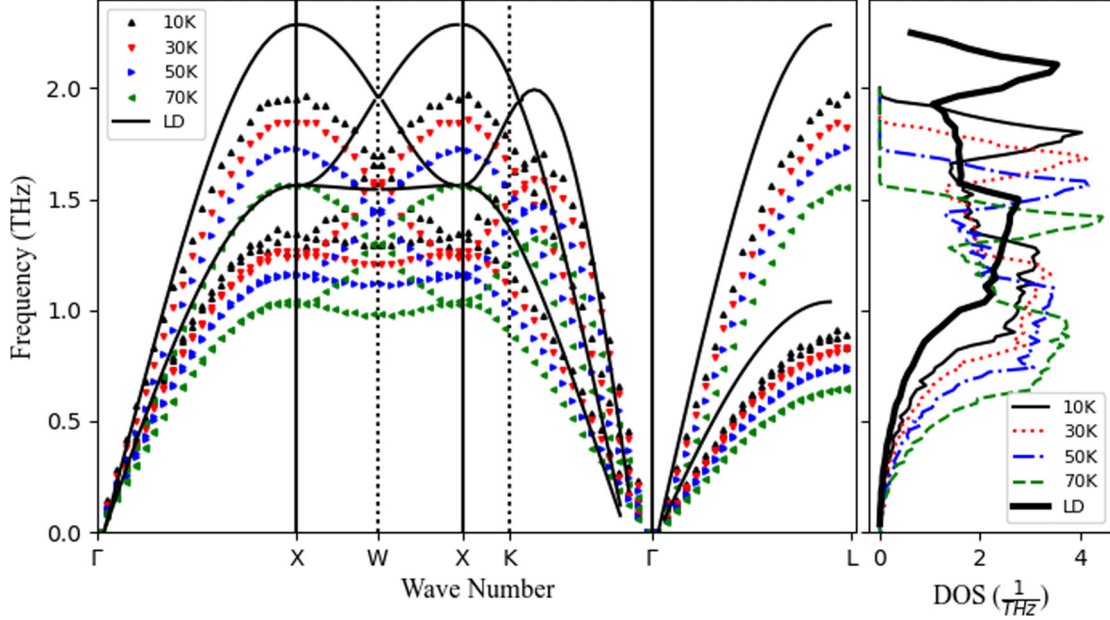
FIG. 3. The PDR curve and the DOS of the argon crystal at four different temperatures. For comparison, the PDR computed using lattice dynamics (LD) is also included.

well minus the calculated kinetic energy (9). The difference between the two positive roots is the displacement magnitude of the atoms from their equilibrium positions. This protocol provides the energy-based definition of amplitude instead of choosing it as an arbitrary parameter,

$$P_{\max} + E_{(tot,D)} = 4\epsilon\left[\left(\frac{\sigma}{r}\right)^{12} - \left(\frac{\sigma}{r}\right)^{6}\right],$$

$$\{r \mid r \geqslant 0 \ \wedge \ \mathrm{Im}(r) \equiv 0\}, \quad R = |r_1 - r_2|. \tag{11}$$

Then we use an algorithm that increases the amplitude of the wave in small steps to get an average of the interatomic distance r equal to the calculated value from Eq. (11). As the perturbation is applied to the z direction only, there is no change in the interatomic distance except for the transverse and longitudinal directions along each string of atoms. As a result, we have no displacement in the x direction.

III. RESULTS AND DISCUSSION

We used the method developed by Kong *et al.* [28,30] to generate the wave-vector frequency structure of the argon crystal (Fig. 3). For comparison and validation, we calculated and added the lattice-dynamics-based dispersion; the data were created using the GULP package [39]. We have also compared our result for one temperature with the experimental data [40] to confirm the data calculated by Kong's method [Fig. 1(c)]. The comparison showed an acceptable match within the statistical limit, which will be discussed below.

The numerical oscillations showed a maximum of $\sim$7.7% change in the results [Fig. 4(a)], which is significantly smaller than the pronounced temperature dependence of frequency under the NPT ensemble. The NVT results also provided intact frequencies for most of the frequency interval and under all four temperature conditions [Fig. 4(b)]. We observed slight changes beyond the statistical oscillation in the PDR at high

frequencies, which are not lattice constant related and contradictory to our assumption of lattice constant dependence of the PDR. Occelli *et al.* showed the dependence of phonon frequencies on many-body terms in potential functions for argon [41]. The many-body terms are absent in the Lennard-Jones potential used in the present work, thus the effect on frequencies [Fig. 4(b)]. The statistical variations observed at NVT provided evidence that the decreasing trend observed in the frequencies as a function of temperature is not an artifact of statistical variations.

A. Importance of the temperature- and energy-dependent definition of a wave packet

Based on the presented data, we have confidence in the observed temperature dependence in our simulations because of the lattice expansion, as suggested by the existing experimental data [33]. Using the PDR and DOS data, we could create wave packets and compare the frequency space of the system, considering the temperature dependence and ignoring it. To structure our validation system with the required temperature-induced lattice constant, we captured the lattice constants after the expansion by relaxing our validation system at each temperature. The resulting lattice constants are listed in Table I, where we also compare the results with the experimental values [42]. The computed lattice constants are in good agreement with the experimental work. We see deviations at higher temperature, which we attribute to the absence of many-body terms in the potential [41], as the terms provide more constraint on the atom motions, thus limiting the lattice constant at high temperatures. The wave-packet validation process is performed in the validation system and under the conditions explained in Sec. II. The simulation results show the importance of the consideration of the temperature dependence of the PDR and DOS in defining a wave packet. Neglecting this dependence results in frequencies that are not
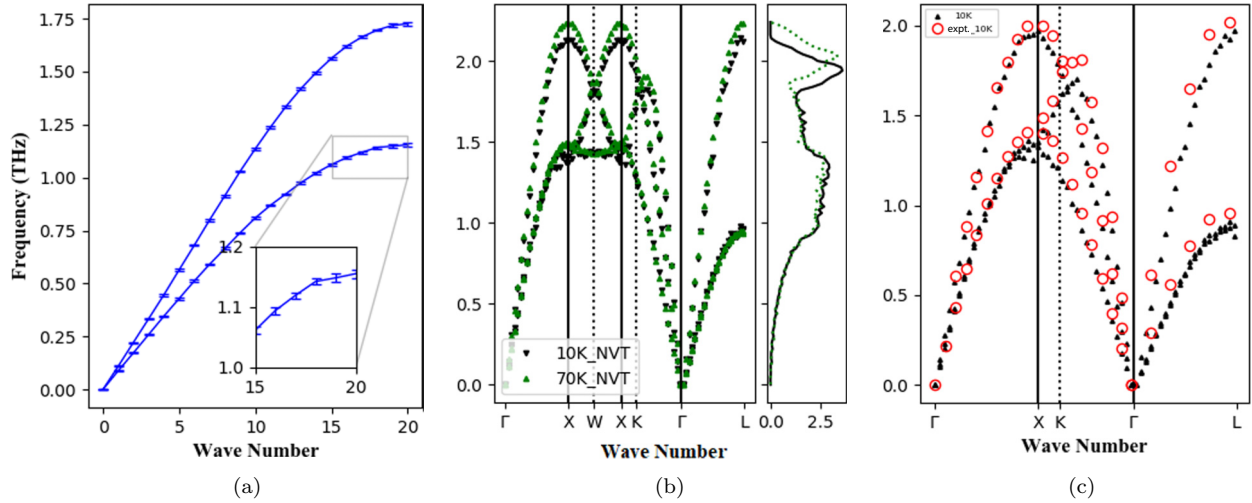
FIG. 4. (a) Uncertainty in frequency analysis. The inset shows a close-up for better visibility. (b) The NVT results showing a slight difference in frequency at high frequencies. The NVT results at 50 and 30 K are not presented for the clarity. (c) Comparison between the PDR resulted from a Green's-function approach and experimental work [40] at 10 K. The red circles are the experimental data and the black triangles are the computational data.

the correct frequencies in the system (see Fig. 5; compare the arrows with the dotted lines). The 0 K frequencies for the same wave vectors are shown in Fig. 5. The 0 K frequencies are commonly used in interpreting the results of phonon dynamics simulations. The arrows are coded with the colors assigned to each temperature. In comparing the location of the arrows with the targeted frequencies (dashed vertical lines) we notice the increase in the gap between them with increasing temperature. The observation emphasizes the importance of the temperature dependence at higher temperatures. We also compare the expected frequencies from the PDR analysis with what we observed in our wave-packet simulations. At 10 K the wave number (right side of each plot) and the frequencies (left side of each plot) match the expected values (solid Gaussian for the wave numbers and dashed line for frequencies) [Fig. 5(a)]. The matching trend continues for both 30 and 50 K except for minimal deviations at the expected frequencies, which we attribute to the uncertainty in the first method used in this work [Figs. 5(b) and 5(c)]. The 70 K data do not show deviations, but we observed low peaks at the target frequencies due to large peaks at low frequencies, which are due to decay to low frequencies. We could not avoid the decay as the fast Fourier transform resolution is dependent on the length of the data set; hence the decay was inevitable [Fig. 5(d)]. At 70 K we observed nonzero spatial frequency values, 2σ-3σ away from the expected maximum, which we attribute to the

low frequency-space resolution in the spatial Fourier analysis. The low number of atoms (60) along the y axis is the reason for low spatial frequency resolution and can be solved by choosing a more computationally extensive system. Nevertheless, we were able to target a frequency with a specific wave vector and show the importance of the temperature-dependent definition of a wave packet.

B. Frequency-based validation of MD simulations

Molecular-dynamics simulations do not represent the quantum particle character of phonons due to their classic nature and the misrepresentation is pronounced more at temperatures well below the Debye temperature, where the quantum effects dominate [43,44] and the classical molecular dynamics can overpredict the frequency contribution to the specific heat. The quantum effects specifically for an argon crystal of particles are mentioned heuristically to be important in a range between one-tenth [43] and one-quarter of the Debye temperature [45]. The wave-packet method as a frequency-specified method and with the additional energy details provided us the chance to do a frequency-based assessment of MD simulations and develop a frequency-based measure to evaluate the reliability of MD simulations with respect to temperature. As a result, we monitored the oscillation of the total kinetic energy (shaded region in Fig. 6) in the simulation and compared the results with the calculated (expected) energy [Eqs. (9) and (10)] for all four frequencies and all four temperature data points (Fig. 6). At 10 K, we observed that the first four frequencies (0.2, 0.4, 0.6, and 0.8 THz) lie within the trend of oscillations of the MD-calculated kinetic energy [Fig. 6(a)]. The last data point falls beyond the MD oscillation band due to the overprediction of the contribution of the frequency at 10 K (Fig. 3). The data show that the kinetic energy calculated by the MD code is reliable at temperatures as low as one-eighth of the Debye temperature of solid argon [46,47] and up to a frequency of 1 THz. This observation is a more exact reliability limit for MD

TABLE I. Lattice constant values from computational work a_{comp} and a comparison with the experimental a_{expt} values (from [42]).

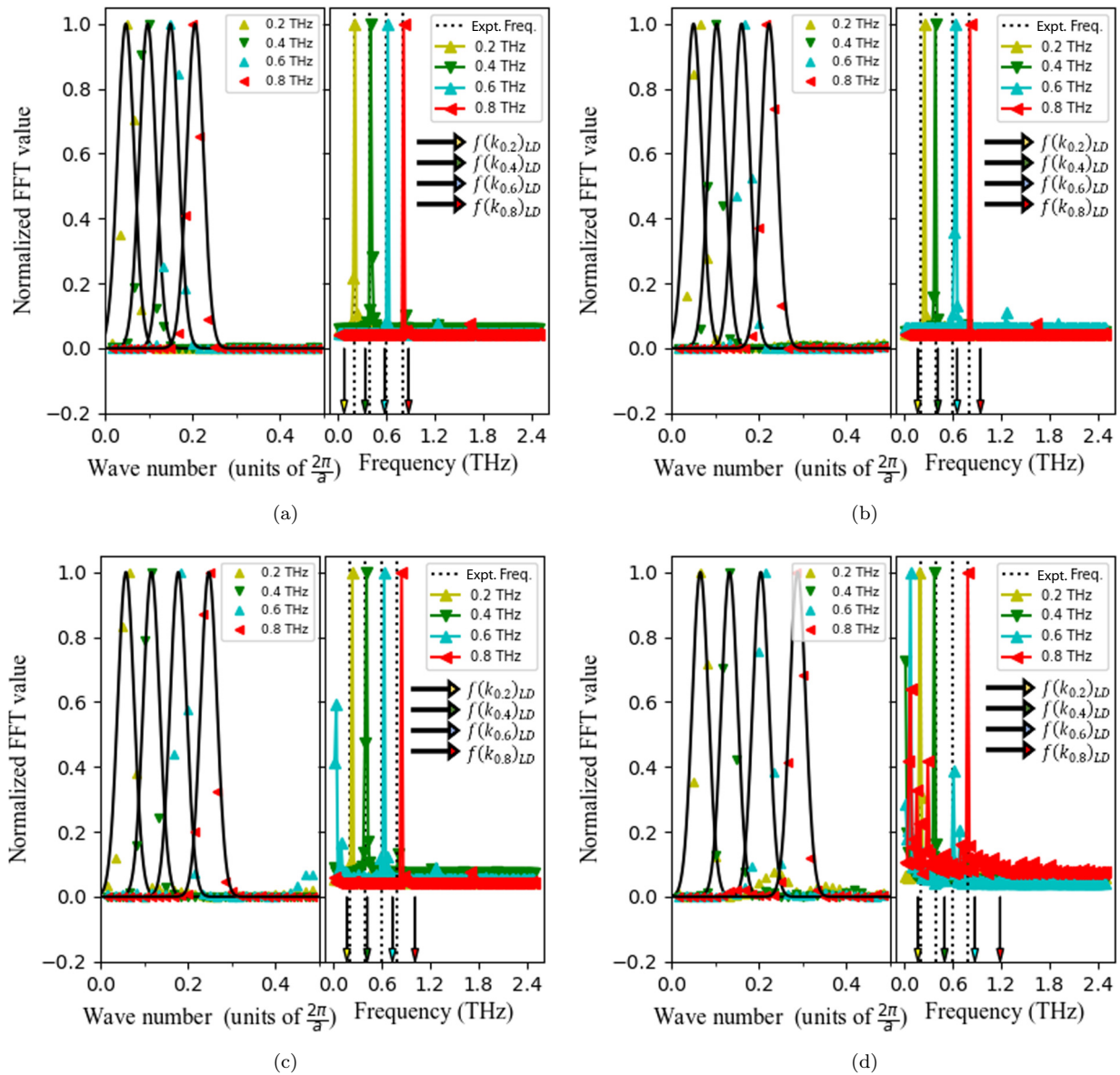| Temperature (K)	Lattice constant (Å)	$\frac{a_{comp}-a_{expt}}{a_{expt}} \times 100$ (%)
0	5.24	
10	5.29	0.2
30	5.33	0.2
50	5.39	0.75
70	5.46	0.92

FIG. 5. Spatial Fourier validation of (a) and (c) the perturbation and (b) and (d) the temporal Fourier validation for four different frequencies at (a) 10 K, (b) 30 K, (c) 50 K, and (d) 70 K. The arrows are the 0 K frequencies that are commonly used in the interpretation of the wave-packet simulations. The arrows are color coded with the colors used for each temperature.

simulations in comparison with the previous ones [43,45]. At 30, 50, and 70 K we observed that the expected data points follow the trend of the MD oscillations. The decline in the 1 THz point for 70 K does not refute the energy definition of MD at 70 K yet still illustrates the importance of the DOS in the definition of the the kinetic energy, which is an important concern at low temperatures.

The quantum definition of the energy used in this work cannot be represented with MD simulations. Consequently, we find the expected value of the energy on the bottom of the energy oscillation at high frequencies of low temperatures, which is due to the consideration of the density of states in the calculations. The observation matches the calculation much better at high temperatures, where the calculated energy is near the maximum of oscillations. We expected the midpoint of the oscillation to match the quantum particle-based energy

calculation, as the calculated energy was added to the system with an algorithm setting the average atomic displacement to the calculated value. As a result, the MD simulations can be a close estimate of a dielectric material even at low temperatures for low frequencies; at high frequencies of high temperature where the DOS decreases rapidly, the MD energy loses the quantum energy trend but its oscillation still enfolds the quantum value.

It is also necessary to address the current concerns about the acoustic wave picture of phonons. Henry and Seyf proposed a different definition, as an extension of the concept defined by Allan *et al.* [48], of lattice vibration with the existence of impurities in materials and raised concerns about the limit of the acoustic wave assumptions of phonon behavior [49]. Although the phonon dynamics provides valuable results, the concern raises questions about the limits in which
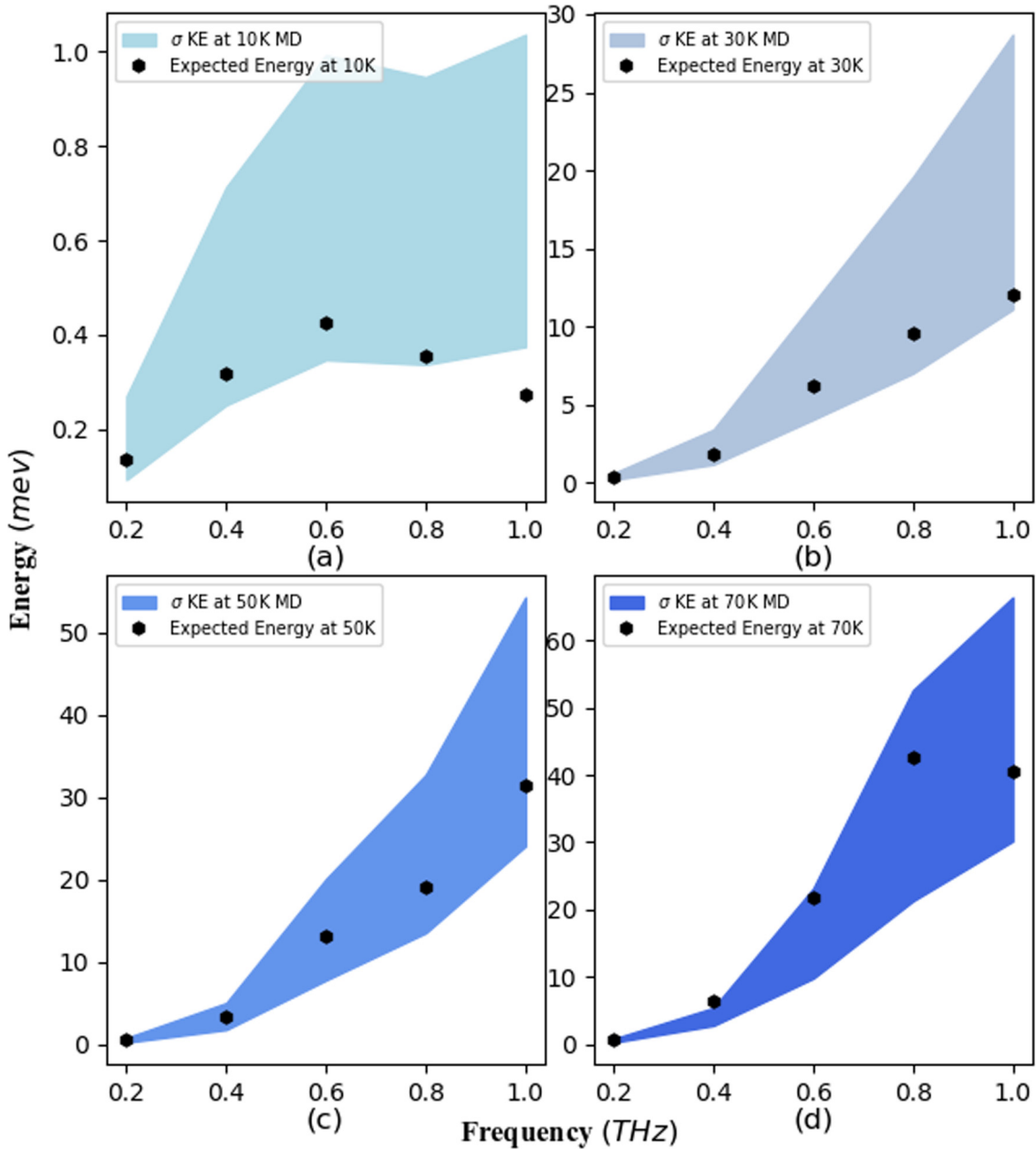
FIG. 6. Energy oscillation of the simulation (shaded area) compared to the energy calculated for each temperature calculated based on the quantum particle picture of the problem (black hexagons) at (a) 10 K, (b) 30 K, (c) 50 K, and (d) 70 K.

this method can provide reliable results. Considering the nature of this work, which is evaluating the dynamics of phonons within a pure crystalline material, this method distances itself from this criticism.

IV. CONCLUSION

In this work we introduced an extension of the phonon dynamics method. The method has always been used disregarding the temperature-dependent PDR and DOS, under which the wave packet is evolving, and the amount of energy a wave packet carries. We utilized a Green's-function-based approach to capture the temperature dependence of the PDR and the DOS and compared wave packets in two cases, one that neglects the temperature dependence and uses the lattice

dynamics (0 K) results and another in which the temperature dependence is considered. The difference in the frequency space of a system considering the temperature dependence and the one using 0 K results was shown and we discovered that its importance increases at higher temperatures, making the consideration more important. Consideration of the temperature-dependent PDR and DOS enabled the definition of the wave-packet amplitude as a parameter that specifies the amount of energy a wave packet carries. As a result, we improved the phonon dynamics method that considers the amplitude of the wave as an arbitrary parameter while considering the amplitude as a tuning knob of the energy. Finally, we were able to use the method to improve a heuristic rule for the validity of MD simulations considering their classical nature and provide a quantitative measure in frequency space for the

matter. The result of the last part of our work provided the result that, at high temperatures, although the MD simulations under a thermostated and equilibrated condition are able to reproduce the correct DOS, they are unable to do so with a frequency band in a system expanded to the lattice constant of high temperatures, resulting in the lost of the energy trend at high frequencies at high temperatures. In contrast, despite the common belief that at low temperatures the MD simulations are not able to provide acceptable results in comparison with the quantum picture of vibrations, they still provide reliable results at temperatures as low as the one-eighth of the Debye temperature and up to 1 THz in the argon case.

[1] A. Jain, S. P. Ong, G. Hautier, W. Chen, W. D. Richards, S. Dacek, S. Cholia, D. Gunter, D. Skinner, G. Ceder, and K. A. Persson, Commentary: The materials project: A materials genome approach to accelerating materials innovation, APL Mater. **1**, 011002 (2013).

[2] D. G. Cahill, P. V. Braun, G. Chen, D. R. Clarke, S. Fan, K. E. Goodson, P. Keblinski, W. P. King, G. D. Mahan, A. Majumdar, H. J. Maris, S. R. Phillpot, E. Pop, and L. Shi, Nanoscale thermal transport. II. 2003–2012, Appl. Phys. Rev. **1**, 011305 (2014).

[3] D. G. Cahill, W. K. Ford, K. E. Goodson, G. D. Mahan, A. Majumdar, H. J. Maris, R. Merlin, and S. R. Phillpot, Nanoscale thermal transport, J. Appl. Phys. **93**, 793 (2003).

[4] M. Maldovan, Phonon wave interference and thermal bandgap materials, Nat. Mater. **14**, 667 (2015).

[5] D. Singh, J. Y. Murthy, and T. S. Fisher, Effect of phonon dispersion on thermal conduction across Si/Ge interfaces, J. Heat Transfer **133**, 122401 (2011).

[6] W. Lv and A. Henry, Direct calculation of modal contributions to thermal conductivity via Green-Kubo modal analysis, New J. Phys. **18**, 013028 (2016).

[7] N. Mingo, Anharmonic phonon flow through molecular-sized junctions, Phys. Rev. B **74**, 125402 (2006).

[8] P. E. Hopkins, Multiple phonon processes contributing to inelastic scattering during thermal boundary conductance at solid interfaces, J. Appl. Phys. **106**, 013528 (2009).

[9] Y. Chalopin and S. Volz, A microscopic formulation of the phonon transmission at the nanoscale, Appl. Phys. Lett. **103**, 01602 (2013).

[10] P. K. Schelling, S. R. Phillpot, and P. Keblinski, Phonon wave-packet dynamics at semiconductor interfaces by molecular-dynamics simulation, Appl. Phys. Lett. **80**, 2484 (2002).

[11] M. Shen, P. K. Schelling, and P. Keblinski, Heat transfer mechanism across few-layer graphene by molecular dynamics, Phys. Rev. B **88**, 045444 (2013).

[12] Z. Wei, Y. Chen, and C. Dames, Wave packet simulations of phonon boundary scattering at graphene edges, J. Appl. Phys. **112**, 024328 (2012).

[13] P. K. Schelling, S. R. Phillpot, and P. Keblinski, Kapitza conductance and phonon scattering at grain boundaries by simulation, J. Appl. Phys. **95**, 6082 (2004).

[14] C. H. Baker, D. A. Jordan, and P. M. Norris, Application of the wavelet transform to nanoscale thermal transport, Phys. Rev. B **86**, 104306 (2012).

[15] T. Hori, Verification of the phonon relaxation time approximation by probing the relaxation process of a single excited mode, Phys. Rev. B **100**, 214116 (2019).

[16] E. S. Landry and A. J. H. McGaughey, Effect of interfacial species mixing on phonon transport in semiconductor superlattices, Phys. Rev. B **79**, 075316 (2009).

[17] J. Callaway, Model for lattice thermal conductivity at low temperatures, Phys. Rev. **113**, 1046 (1959).

[18] G. Chen, M. Neagu, and T. Borca-Tasciuc, Thermal conductivity and heat transfer in superlattices, MRS Proc. **478**, 85 (1997).

[19] C. Jeong, S. Datta, and M. Lundstrom, Full dispersion versus Debye model evaluation of lattice thermal conductivity with a Landauer approach, J. Appl. Phys. **109**, 073718 (2011).

[20] Z. Aksamija and I. Knezevic, Lattice thermal conductivity of graphene nanoribbons: Anisotropy and edge roughness scattering, Appl. Phys. Lett. **98**, 141919 (2011).

[21] Y. Wang, Temperature-dependent phonon dispersion relation in magnetic crystals, Solid State Commun. **54**, 279 (1985).

[22] J. M. Hastings, J. P. Pouget, G. Shirane, A. J. Heeger, N. D. Miro, and A. G. MacDiarmid, One-Dimensional Phonons and "Phase-Ordering" Phase Transition in $Hg_{3-\delta}AsF_6$, Phys. Rev. Lett. **39**, 1484 (1977).

[23] J. D. Axe, J. Harada, and G. Shirane, Anomalous acoustic dispersion in centrosymmetric crystals with soft optic phonons, Phys. Rev. B **1**, 1227 (1970).

[24] K. Tajima, Y. Endoh, and Y. Ishikawa, Acoustic-Phonon Softening in the Invar Alloy Fe_3Pt, Phys. Rev. Lett. **37**, 519 (1976).

[25] J. Hone, in *Carbon Nanotubes: Synthesis, Structure, Properties, and Applications*, edited by M. S. Dresselhaus, G. Dresselhaus, and P. Avouris, Topics in Applied Physics Vol. 80 (Springer, Berlin, 2001), pp. 273–286.

[26] A. Savin, B. Hu, and Y. Kivshar, Thermal conductivity of single-walled carbon nanotubes, Phys. Rev. B **80**, 195423 (2009).

[27] M. D. Gerboth and D. G. Walker, Effects of acoustic softening on thermal conductivity beyond group velocity, J. Appl. Phys. **127**, 204302 (2020).

[28] L. T. Kong, G. Bartels, C. Campañá, C. Denniston, and M. H. Müser, Implementation of Green's function molecular dynamics: An extension to LAMMPS, Comput. Phys. Commun. **180**, 1004 (2009).

[29] P. Heino, Dispersion and thermal resistivity in silicon nanofilms by molecular dynamics, Eur. Phys. J. B **60**, 171 (2007).

[30] L. T. Kong, Phonon dispersion measured directly from molecular dynamics simulations, Comput. Phys. Commun. **182**, 2201 (2011).

[31] S. Plimpton, Fast parallel algorithms for short-range molecular dynamics, J. Comput. Phys. **117**, 1 (1995).

[32] P. Tan, Y. Deng, and Q. Zhao, Temperature-dependent Raman spectra and anomalous Raman phenomenon of highly oriented pyrolytic graphite, Phys. Rev. B **58**, 5435 (1998).

[33] Y. Yun, D. Legut, and P. M. Oppeneer, Phonon spectrum, thermal expansion and heat capacity of UO$_2$ from first principles, J. Nucl. Mater. **426**, 109 (2012).

[34] S. G. Popov, J. J. Carbajo, V. K. Ivanov, and G. L. Yoder, Thermophysical properties of MOX and UO$_2$ fuels including the effects of irradiation, Oak Ridge National Laboratory Report No. ORNL/TM-2000/351, 2000 (unpublished).

[35] A. J. H. McGaughey and M. Kaviany, Thermal conductivity decomposition and analysis using molecular dynamics simulations. Part I. Lennard-Jones argon, Int. J. Heat Mass Transf. **47**, 1783 (2004).

[36] N. W. Ashcroft and N. D. Mermin, *Solid State Physics* (Saunders, Philadelphia, 1967), pp. 398–400.

[37] J. P. Wolfe, *Imaging Phonons: Acoustic Wave Propagation in Solids* (Cambridge University Press, Cambridge, 2005).

[38] K. C. Sood and M. K. Roy, Longitudinal phonons and high-temperature heat conduction in germanium, J. Phys.: Condens. Matter **5**, 301 (1993).

[39] J. Gale and A. L. Rohl, The general utility lattice program (GULP), Mol. Simul. **29**, 291 (2003).

[40] Y. Fuji, N. A. Lurie, R. Pynn, and G. Shirane, Inelastic neutron scattering from solid Ar, Phys. Rev. B **10**, 3647 (1974).

[41] F. Occelli, M. Krisch, P. Loubeyre, F. Sette, R. Le Toullec, C. Masciovecchio, and J.-P. Rueff, Phonon dispersion curves in an argon single crystal at high pressure by inelastic x-ray scattering, Phys. Rev. B **63**, 224306 (2001).

[42] O. G. Peterson, D. N. Batchelder, and R. O. Simmons, Measurements of x-ray lattice constant, thermal expansivity, and isothermal compressibility of argon crystals, Phys. Rev. **150**, 703 (1966).

[43] A. J. H. McGaughey and M. Kaviany, Phonon transport in molecular dynamics simulations: Formulation and thermal conductivity prediction, Adv. Heat Transfer **39**, 169 (2006).

[44] A. J. H. McGaughey and M. Kaviany, Observation and description of phonon interaction in molecular dynamics simulations, Phys. Rev. B **71**, 184305 (2005).

[45] N. Roberts, D. Walker, and D. Li, Molecular dynamics simulation of thermal conductivity of nanocrystalline composite films, Int. J. Heat Mass Transf. **52**, 2002 (2008).

[46] R. H. Beaumont, H. Chihara, and J. A. Morrison, Thermodynamic properties of krypton. vibrational and other properties of solid argon and solid krypton, Proc. Phys. Soc. **78**, 1462 (1961).

[47] J. D. Launay, Measurements of x-ray lattice constant, thermal expansivity, and isothermal compressibility of argon crystals, J. Chem. Phys. **22**, 1676 (1954).

[48] P. B. Allen, J. L. Feldman, J. Fabian, and F. Wooten, Diffusons, locons and propagons: Character of atomic vibrations in amorphous Si, Philos. Mag. B **79**, 1715 (1999).

[49] H. R. Seyf, L. Yates, T. L. Bougher, S. Graham, B. A. Cola, T. Detchprohm, M.-H. Ji, J. Kim, R. Dupuis, W. Lv, and A. Henry, Rethinking phonons: The issue of disorder, npj Comput. Mater. **3**, 49 (2017).